JACS
JOURNAL OF THE AMERICAN CHEMICAL SOCIETY

ARTICLE

pubs.acs.org/JACS

Heteroepitaxial Growth of High-Index-Faceted Palladium Nanoshells and Their Catalytic Performance

Feng Wang,[†,§] Chuanhao Li,[‡] Ling-Dong Sun,[*,§] Haoshuai Wu,[§] Tian Ming,[†] Jianfang Wang,[*,†] Jimmy C. Yu,[‡] and Chun-Hua Yan[*,§]

[†]Department of Physics and [‡]Department of Chemistry, The Chinese University of Hong Kong, Shatin, Hong Kong SAR, China

[§]State Key Lab of Rare Earth Materials Chemistry and Applications, Peking University, Beijing 100871, China

Supporting Information

ABSTRACT: The development of high-performance nanocatalysts relies essentially on the generation of stable and active surface sites at the atomic scale through synthetic control of the size, shape, and chemical composition of nanoscale metals and metal oxides. One promising route is to induce the exposure of catalytically active high-index facets of nanostructures through shape-controlled syntheses. We have designed and prepared two types of Pd nanoshells that are enclosed by high-index {730} and {221} facets through heteroepitaxial growth on high-index-faceted Au nanocrystals. The turnover numbers per surface atom of the high-index-faceted Pd nanoshells have been found to be 3−7 times those of Pd and Au−Pd core−shell nanocubes that possess only {100} facets in catalyzing the Suzuki coupling reaction. These results open up a potential for the development of inexpensive and highly active metal nanocatalysts.

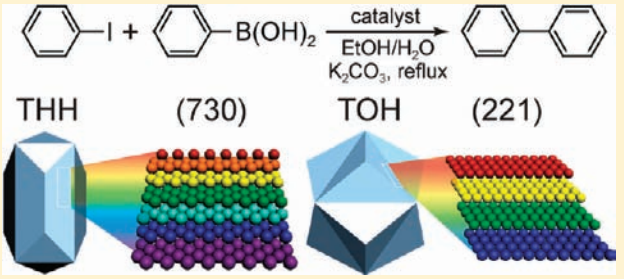

INTRODUCTION

One of the major goals in current catalysis research is to design more efficient, stable, and economical nanocatalysts for efficient energy utilization, chemical production, and pollution control.[1−5] The development of these next-generation nanocatalysts relies on generating stable and active surface sites at the atomic scale[6−13] through synthetic approaches for the control of the size, shape, and chemical composition of nanocatalysts.[14−19] Fundamental studies on the single-crystalline surfaces of bulk Pt have shown that high-index planes exhibit a high density of atomic steps, ledges, and kinks, which usually serve as active sites with high catalytic activities.[20] Consequently, tailoring the exposure of high-index facets through shape-controlled syntheses is a potential route for the fabrication of efficient next-generation nanocatalysts.

Palladium is widely used in areas ranging from fuel cells, hydrogen storage, water treatment, and hydrogen purification. Pd nanoparticles function as indispensable catalysts in petroleum cracking, hydrogenation, organic reactions, and low-temperature reduction of automobile pollutants. Previous catalytic studies have so far focused dominantly on nearly spherical Pd nanoparticles with ill-defined facets, which prevent from quantitative measurements of the catalytic performance of different facets. We chose to study the effect of different facets on the catalytic performance of Pd nanocrystals. To date, chemical methods have been recently developed for the growth of high-index-faceted tetrahexahedral (THH)[21] and trisoctahedral (TOH)[22,23] Au nanocrystals in solutions in high yields and large quantities, while only electrochemical methods have been demonstrated for the preparation of THH Pd[24] and Pt[25] nanocrystals on electrodes. In addition, Au nanocubes have been employed in a recent experiment to direct the growth of THH Au−Pd core−shell nanocrystals.[26]

In this Article, we report the design and preparation of two types of Pd nanoshells that are enclosed by high-index {730} and {221} facets, respectively. THH and TOH Au nanocrystals are employed as the core supports to direct the growth of the high-index-faceted Pd nanoshells. The catalytic performance of these high-index-faceted Pd nanoshells for the Suzuki coupling reaction was measured and compared to those of Pd and Au−Pd core−shell nanocubes that possess only {100} facets. The turnover numbers (TONs) per surface atom of the high-index-faceted Pd nanoshells are 3−7 times those of the Pd and Au−Pd core−shell nanocubes. These results demonstrate that high-index-faceted nanocrystals are excellent nanocatalytic systems for organic reactions and surface chemical processes, allowing us to push the envelope in the development of more efficient and stable catalysts for the fuel industry.

EXPERIMENTAL SECTION

Preparation of the THH Au−Pd Core−Shell Nanocrystals.

The growth of the THH Au nanocrystals followed a described procedure.[21] The THH Au−Pd core−shell nanocrystals were grown through a seed-mediated method. Typically, the THH Au nanocrystal solution (1 mL) was added into an aqueous growth solution composed

Received: October 25, 2010
Published: December 21, 2010

dx.doi.org/10.1021/ja1095733 | J. Am. Chem. Soc. 2011, 133, 1106–1111

of cetyltrimethylammonium bromide (CTAB, 0.025 M, 4 mL), H_2PdCl_4 (0.01 M, 0.015 mL), and ascorbic acid (0.1 M, 0.008 mL). The reaction mixture was mixed by gentle inversion for 10 s and then left undisturbed overnight at room temperature. The resultant solution was centrifuged at 6300*g* for 10 min, and the precipitate was redispersed in water (1 mL) for the catalytic reaction. The THH Pd nanoshells with different thicknesses were prepared similarly by changing the volume of the H_2PdCl_4 solution to 0.005, 0.010, and 0.020 mL. The corresponding volumes of the ascorbic acid solution were 0.003, 0.005, and 0.010 mL, respectively. The percentage of H_2PdCl_4 consumed for the shell growth was measured to be (73 ± 4)% using an inductively coupled plasma atomic emission spectroscopy (IRIS Advantage, Thermo Jarrell Ash Corp.).

Preparation of the TOH Au−Pd Core−Shell Nanocrystals. The preparation of the TOH Au−Pd core−shell nanocrystals was realized through three seed-mediated growth steps. Au octahedra were prepared in the first step, following a reported method.[27] In a typical growth, an aqueous $HAuCl_4$ solution (0.01 M, 0.25 mL) was first mixed with a CTAB solution (0.1 M, 9.75 mL). A freshly prepared, ice-cold $NaBH_4$ solution (0.01 M, 0.60 mL) was then added under vigorous stirring. The resultant seed solution was kept under gentle stirring for 3 h at room temperature before use. The seed solution was diluted 10 times, and the diluted seed solution (0.12 mL) was added to a mixture solution made of CTAB (0.1 M, 4 mL), water (19 mL), $HAuCl_4$ (0.01 M, 0.40 mL), and ascorbic acid (0.1 M, 1.5 mL). The reaction mixture solution was mixed by gentle inversion for 10 s and then left undisturbed overnight at room temperature. The TOH Au nanocrystals were prepared in the second step, where the Au octahedra were used as the seeds. Briefly, the as-grown Au octahedron solution (2.5 mL) was added into an aqueous growth solution composed of cetyltrimethylammonium chloride (CTAC, 0.025 M, 30.3 mL), $HAuCl_4$ (0.01 M, 0.5 mL), and ascorbic acid (0.1 M, 0.25 mL). The obtained solution was mixed by gentle inversion for 10 s and then left undisturbed overnight at room temperature. The resultant TOH nanocrystal solution (30 mL) was centrifuged at 6300*g* for 10 min, and the precipitate was redispersed into an aqueous CTAB solution (0.1 M, 10 mL) for the further growth. The growth of the TOH Au−Pd core−shell nanocrystals was similar to that of the THH Au−Pd core−shell nanocrystals, where the THH Au nanocrystal solution was replaced with the TOH Au nanocrystal solution.

Growth of the Pd Nanocubes. The growth of the Pd nanocubes was according to a reported procedure.[28] Briefly, an aqueous H_2PdCl_4 solution (0.01 M, 0.5 mL) was first added into an aqueous CTAB solution (0.0125 M, 10 mL). The mixture solution was then heated to 96 °C and kept at this temperature for 20 min, followed by the addition of an aqueous ascorbic acid solution (0.1 M, 0.08 mL). The resultant solution was kept at the same temperature for another 30 min for the nanocube growth. The percentage of H_2PdCl_4 consumed for the nanocube growth was measured to be (65 ± 3)%.

Growth of the Au−Pd Core−Shell Nanocubes. The Au−Pd core−shell nanocubes were grown using the Au octahedra above as the seeds. Specifically, the as-grown Au octahedron solution (1 mL) was added into an aqueous growth solution composed of CTAB (0.025 M, 4 mL), H_2PdCl_4 (0.01 M, 0.16 mL), and ascorbic acid (0.1 M, 0.08 mL). The reaction mixture solution was mixed by gentle inversion for 10 s and then left undisturbed overnight at room temperature. The percentage of H_2PdCl_4 consumed for the shell growth was measured to be (73 ± 4)%.

Operation of the Suzuki Coupling Reaction. The Suzuki coupling reaction between phenylboronic acid and iodobenzene was performed with the THH and TOH Au−Pd core−shell nanocrystals prepared from 0.015 mL of the H_2PdCl_4 solution. Specifically, iodobenzene (0.034 mL, 0.3 mmol) was added to ethanol (4 mL) in the presence of phenylboronic acid (0.073 g, 0.6 mmol), K_2CO_3 (0.138 g, 1 mmol), and the nanocrystal solution (1 mL). The mixture was placed in an oil bath at 85 °C under gentle stirring for 1 h. The product was extracted with CH_2Cl_2 and directly analyzed by gas chromatography−mass spectrometry (GC−MS). The GC−MS analysis was performed on an HP 6890 GC system equipped with an HP 5973 mass-selective detector and an HP-5 MS capillary column. The control experiments were carried out with the same procedure, except that the different nanocrystals were utilized.

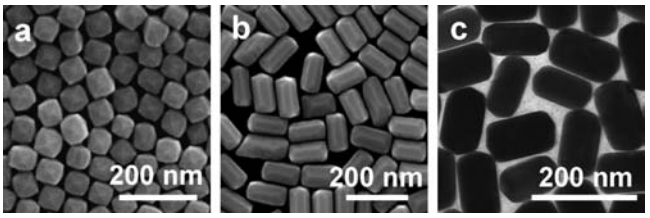

Figure 1. (a,b) SEM images of the THH Au nanocrystals at different orientations. (c) TEM image of the THH Au nanocrystals.

Nanocrystal Structure Characterization. Transmission electron microscopy (TEM) imaging was performed on an FEI CM120 microscope. High-resolution (HR) TEM and high-angle annular dark-field (HAADF)-scanning transmission electron microscopy (STEM) characterizations were carried out on an FEI Tecnai F20 microscope equipped with an Oxford energy-dispersive X-ray analysis system. Scanning electron microscopy (SEM) images were acquired on an FEI Quanta 400 FEG microscope.

RESULTS AND DISCUSSION

Structure Characterizations. The underlying principle of building a high-index-faceted Pd nanoshell is to deposit Pd atoms heteroepitaxially onto pregrown high-index-faceted THH and TOH Au nanocrystals through a reduction reaction in solutions. Previously demonstrated methods of epitaxially growing Pd shells on Au nanorods and octahedra to produce Au−Pd core−shell cuboids[29] and nanocubes,[27,30] respectively, in aqueous CTAB solutions were adapted for the preparation of high-index-faceted Pd nanoshells. Because Pd nanocrystals are usually enclosed with {100} facets in aqueous CTAB solutions,[27,29,30] thin Pd shells were grown so that the THH and TOH shapes with high-index facets could be maintained.

The THH Au nanocrystals were prepared using a seeded growth method.[21] They are elongated and have an average diameter and length of 71 ± 8 and 125 ± 12 nm, respectively (Figure 1 and Figure S1, Supporting Information). They are enclosed with 24 {730} facets, which have been characterized previously by us in detail.[21]

The growth of a thin Pd shell enlarged the nanocrystals. The final shape of the resultant Au−Pd core−shell nanocrystals is dependent on the thickness of the Pd shell, and it was in turn controlled by the supplied amount of the Pd precursor (Figures S2 and S3, Supporting Information). The core−shell nanocrystals with thin Pd shells exhibit clear facets, which are very similar to those of the original elongated THH Au nanocrystals (Figure 2a). As the Pd shell becomes thicker, the core−shell nanocrystals evolve from THH to cuboid shapes. The Pd shell of the Au−Pd core−shell nanocrystals employed in the catalytic study was controlled to be thin. The average diameter and length of the core−shell nanocrystals were measured to be 77 ± 7 and 132 ± 10 nm, respectively (Figure 2b and c). The thickness of the Pd shell is therefore ~3 nm. We carefully characterized the facets and structure of the core−shell nanocrystals. Because a THH nanocrystal can be considered to be derived geometrically from a cuboid that possesses 6 equivalent

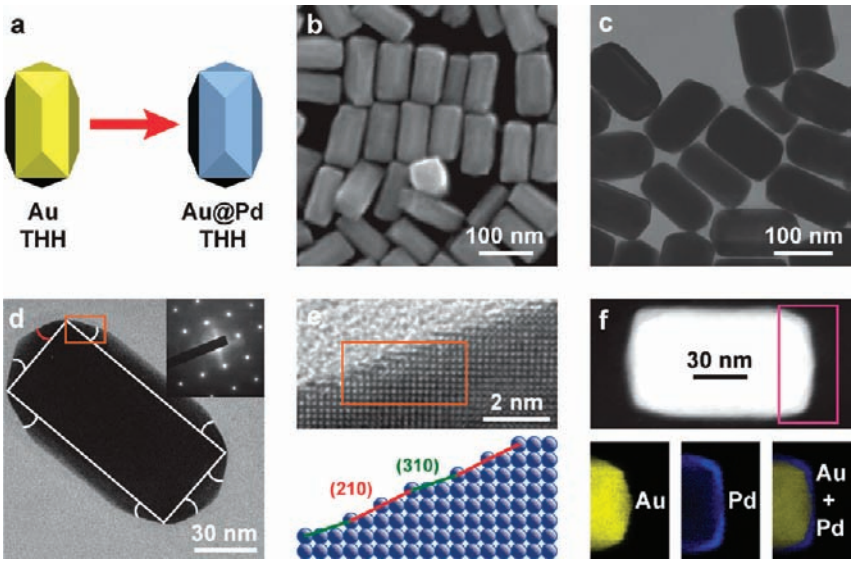

Figure 2. Elongated THH Pd nanoshells. (a) Schematic showing the growth of THH Au−Pd core−shell nanocrystals from THH Au nanocrystals. (b) SEM image. (c) TEM image. (d) TEM image of a single core−shell nanocrystal viewed along the [00−1] axis. Inset: Electron-diffraction pattern recorded on the nanocrystal. (e) Upper: HRTEM image of the region indicated with the orange box in (d). The image has been rotated counterclockwise, with the length axis of the entire nanocrystal aligned horizontally. Lower: Atomic model corresponding to the region indicated with a box in the HRTEM image. (f) Upper: HAADF-STEM image of a single core−shell nanocrystal. Lower: Elemental Au map (left), elemental Pd map (middle), and the merged elemental map (right) acquired in the region indicated with a box in the HAADF-STEM image.

{100} facets, the facet indices of the core−shell nanocrystals can be determined from the angle between the bevel and base planes of the protruding pyramids (Figure 2a and d). The angle can be measured from the TEM image that is recorded along the ⟨100⟩ axis. When a THH nanocrystal is aligned along the ⟨100⟩ axis, 8 out of its 24 facets are visible, and the facets that are parallel to the viewing direction are projected to be straight edges. Electron-diffraction patterns were recorded on the core−shell nanocrystals to align them along the ⟨100⟩ axis (Figure 2d). The angles between the bevel and base planes of the shown THH Au−Pd core−shell nanocrystal were measured to be 22°, 24°, 27°, 23°, 23°, 23°, 23°, and 25°, clockwise, starting from the one indicated in orange, respectively (Figure 2d). An average value of (24 ± 1)° was obtained. This value indicates that the facets on the elongated THH Au−Pd core−shell nanocrystals are high-index {730} planes, because the angle calculated according to {730} facets is 23.2°.

The atomic arrangement of Pd atoms on the facets of the Au−Pd core−shell nanocrystals was further investigated with HRTEM. The facets were seen to be composed of {210} and {310} subfacets (Figure 2e). There are a number of atomic steps on the facets. The core−shell structure was also elucidated unambiguously by elemental mapping under HAADF-STEM. The THH Au nanocrystal core was seen to be coated with a uniform thin Pd shell (Figure 2f). The thinness and uniformity allow the Pd shell to epitaxially inherit the high-index facets from the Au nanocrystal core.

The preparation of TOH Au nanocrystals by reducing $HAuCl_4$ with ascorbic acid in aqueous CTAC solutions has been described before.[22] The TOH Au nanocrystals in our study were prepared using the seeded growth method, which affords high size uniformity and controllability. CTAB-capped Au octahedra[27,30] were utilized as the seeds. The average distance from one apex to the opposite apex of the Au octahedra is 17 ± 1 nm (Figure S4, Supporting Information). The distance from one apex to the opposite apex of the resultant TOH Au nanocrystals is 67 ± 3 nm (Figure 3a and b). HRTEM imaging on the individual nanocrystals

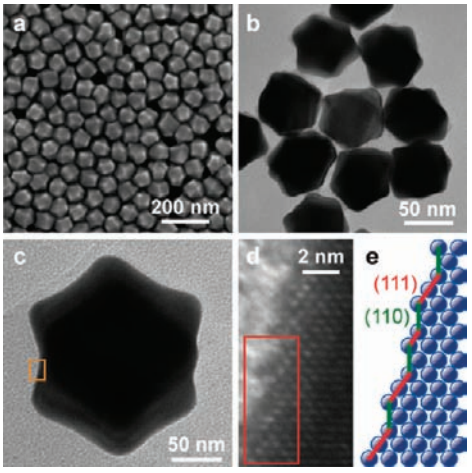

Figure 3. TOH Au nanocrystals. (a) SEM image. (b) TEM image. (c) TEM image of a TOH Au nanocrystal viewed along the [1−10] axis. (d) HRTEM image of the region indicated by the orange rectangle in (c). (e) Two-dimensional lattice model illustrating the high-index (221) facet. The model corresponds to the region indicated by the red rectangle in (d).

that are oriented along the [1−10] axis shows that they are enclosed with high-index {221} facets (Figure 3c−e). Each {221} facet is composed of {111} and {110} subfacets. These structural observations are consistent with those reported previously.[22]

The heteroepitaxial growth of a Pd shell on the TOH Au nanocrystals (Figure 4a) followed the same procedure as that on the THH Au nanocrystals. The thickness of the Pd shell increased as the supplied amount of the Pd precursor was increased (Figures S5 and S6, Supporting Information). The average distance from one apex to the opposite apex of the TOH Au−Pd core−shell nanocrystals employed in the catalytic study was measured to be

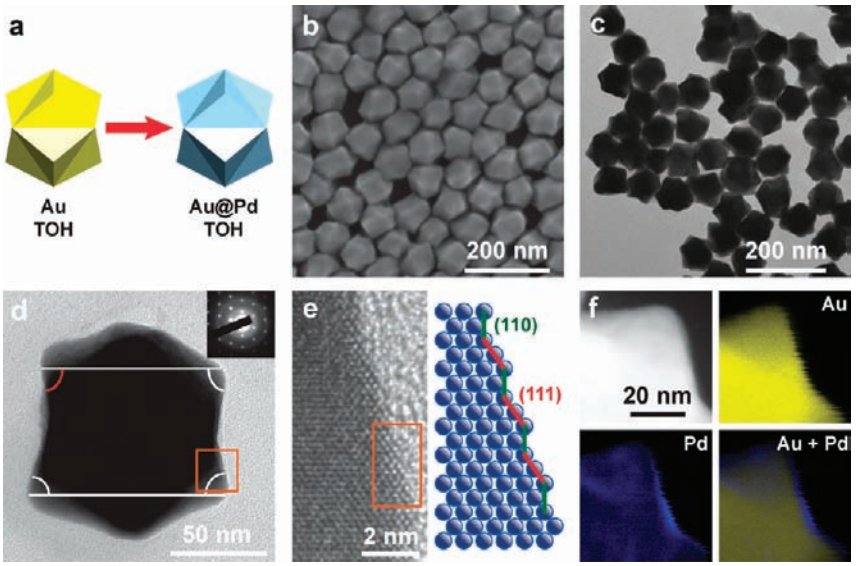

Figure 4. TOH Pd nanoshells. (a) Schematic showing the growth of TOH Au−Pd core−shell nanocrystals from TOH Au nanocrystals. (b) SEM image. (c) TEM image. (d) TEM image of a single Au−Pd core−shell nanocrystal viewed along the [−110] axis. Inset: Electron-diffraction pattern recorded on the nanocrystal. (e) Left: HRTEM image of the region indicated with a box in (d). Right: Atomic model corresponding to the region indicated with a box in the HRTEM image. (f) HAADF-STEM image (top left), elemental Au map (top right), elemental Pd map (bottom left), and the merged elemental map (bottom right) acquired from a part of a TOH core−shell nanocrystal. The imaged region is similar to that shown in (d). The right edge corresponds to a projected high-index facet.

78 ± 5 nm (Figure 4b and c). The thickness of the Pd shell is therefore ~5 nm. When a TOH nanocrystal is aligned along the ⟨110⟩ axis, 10 out of the 24 facets face the viewing direction. Four facets that are parallel to the viewing direction are projected to be straight edges (Figure 4a). The indices of these 4 facets can be determined by measuring the angles formed between them and the {001} planes after the nanocrystal is aligned along the ⟨110⟩ axis with the assistance of electron diffraction (Figure 4d). The angles measured on the shown TOH Au−Pd core−shell nanocrystal are 76°, 78°, 74°, and 73°, clockwise, starting from the one indicated in orange, respectively (Figure 4d). The average value is (75 ± 2)°. This value is close to the angle of 70.5° calculated according to the assumed {221} facets.

The atomic arrangement on the nanocrystal facets was also captured with HRTEM (Figure 4e). The facets were seen to be composed of (110) and (111) subfacets. The geometrical angle measurement results together with the HRTEM characterizations properly suggest that the facets on the TOH Au−Pd core−shell nanocrystal are high-index {221} planes. Elemental mapping under HAADF-STEM imaging revealed the Au−Pd core−shell structure and the presence of a thin Pd shell on the high-index {221} facets (Figure 4f). The combination of all of the structural characterizations unambiguously indicates that the high-index {221} facets have been inherited by the Pd nanoshell from the TOH Au nanocrystal core.

Catalytic Performance in the Suzuki Coupling Reaction. The catalytic behaviors of bulk Pd surfaces and nearly spherical Pd nanoparticles have been studied extensively. Among the diverse catalytic reactions employing Pd-based catalysts, the Suzuki coupling reaction has been recently widely used as a model reaction to test the catalytic performance of Pd nanocrystals of various shapes.[31−33] In this reaction, phenylboronic acid is coupled with iodobenzene to give biphenyl (Figure 5a). This reaction was also selected in our study to investigate the catalytic behaviors of the high-index-faceted Pd nanoshells and compare them with those of

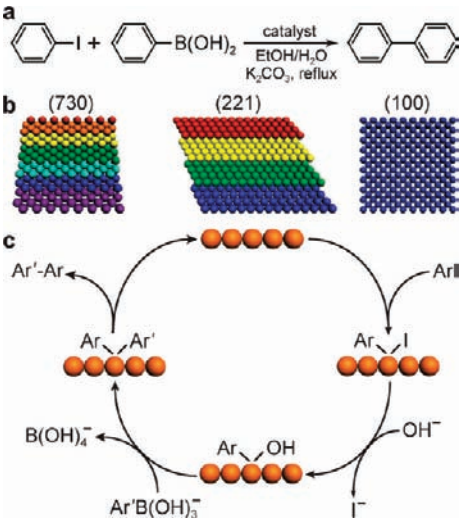

Figure 5. Suzuki coupling reaction between phenylboronic acid and iodobenzene. (a) Reaction equation. (b) Schematic showing the {730}, {221}, and {100} facets that catalyze the reaction. (c) Schematic showing the reaction mechanism on the Pd surface.

low-index-faceted Pd nanocubes and Au−Pd core−shell nanocubes (Figure 5b and c). The use of Au−Pd core−shell nanocubes was to investigate the possible effect of the Au nanocrystal core on the catalytic performance.

The Pd nanocubes are enclosed with the {100} facets. They have an average edge length of 33 ± 3 nm (Figure S7, Supporting Information). The Au−Pd core−shell nanocubes have an average edge length of 47 ± 2 nm. Although their facets are slightly nonflat, they should be very close to the {100} facets (Figure S8, Supporting Information). The Suzuki coupling reaction was carried out under the same conditions three times per catalyst

dx.doi.org/10.1021/ja1095733 |J. Am. Chem. Soc. 2011, 133, 1106–1111

Table 1. Reaction Yields and TONs per Surface Pd Atom of the Pd-Containing Nanocrystal Catalysts

catalyst	yield (%)	number of surface Pd atoms	TON (s^{-1})
THH Pd nanoshells	94 ± 1	4.38×10^{15}	10.8 ± 0.1
recycled THH Pd nanoshells	86	4.38×10^{15}	9.9
TOH Pd nanoshells	96 ± 5	4.03×10^{15}	11.9 ± 0.5
recycled TOH Pd nanoshells	86	4.03×10^{15}	10.7
Pd nanocubes	57 ± 7	6.92×10^{15}	4.2 ± 0.3
Au−Pd core−shell nanocubes	56 ± 10	1.77×10^{16}	1.6 ± 0.2

sample for the four types of Pd-containing nanocrystals. In addition, the coupling reaction was also performed in the presence of the THH Au nanocrystals, the TOH Au nanocrystals, and CTAB, respectively, or without the addition of any extra species. No biphenyl was detected in the latter four reaction runs, which indicates that Pd-containing nanocrystals are indispensable for the coupling reaction to occur. The reaction yields after 1 h of reaction for the four types of Pd-containing nanocrystals are listed in Table 1. In the presence of the THH and TOH Pd nanoshells, 94% and 96% of the iodobenzene reactant was converted into biphenyl, respectively. In comparison, the reaction yields were 57% and 56% when the Pd and Au−Pd core−shell nanocubes were used as the catalysts, respectively. The catalytic efficiencies of the THH and TOH Pd nanoshells are also higher than those of the Pd nanospheres,[31] nanorods,[32] nanobranches,[32] and icosahedra[33] that were utilized previously for the same coupling reaction in terms of the catalyst amount and the reaction time. In those reactions, the molar ratios of the total Pd atoms to iodobenzene were 3%, 1.6%, 1.8%, and 1.7%, respectively, and the reaction time ranged from 4 to 8 h to give reaction yields above 90%. In our experiment, the molar ratio of the total metal atoms to iodobenzene in the reaction was 0.2% for both the THH and the TOH Au−Pd core−shell nanocrystals. If only the Pd atoms are considered, the molar ratio of the total Pd atom to iodobenzene is just 0.05%.

We further calculated the total numbers of the surface Pd atoms of the four types of Pd-containing nanocrystals that were added in the coupling reaction and determined the TONs per surface Pd atom (Table 1). The calculation details are provided in the Supporting Information. The obtained TONs per surface Pd atom are 10.8, 11.9, 4.2, and 1.6 s^{-1} for the THH and TOH Pd nanoshells, and the Pd and Au−Pd core−shell nanocubes, respectively. The TONs of the high-index-faceted Pd nanoshells are 3−7 times those of the low-index-faceted Pd and Au−Pd core−shell nanocubes. Because these TONs have been normalized against the corresponding numbers of the surface Pd atoms, the larger TONs possessed by the Au−Pd core−shell nanocrystals suggest that the high-index {730} and {221} facets exhibit higher catalytic activities than the low-index {100} facets. The higher catalytic activities can be ascribed to the presence of a large number of Pd atoms at steps on the high-index facets. Three-sevenths and one-third of the Pd atoms on the {730} and {221} facets are at steps, while there are no Pd atoms at steps on the {100} facets (Figure 5b). The Pd atoms at steps are more coordinatively unsaturated than those on the flat terraces. They are therefore more catalytically active. In addition, the TON per surface Pd atom of the Au−Pd core−shell nanocubes is about one-half that of the Pd nanocubes. Whether this difference is caused by the presence of the Au nanocrystal core or due to the slightly nonflat facets warrants further investigation.

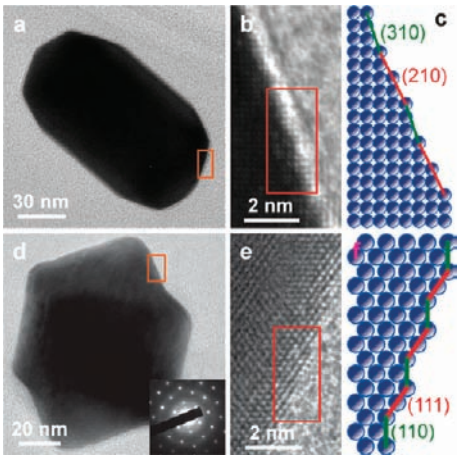

Figure 6. Pd nanoshells after one cycle of the Suzuki coupling reaction. (a) TEM image of a THH Au−Pd core−shell nanocrystal viewed along the [00−1] axis. (b) HRTEM image of the region indicated with the box in (a). The image has been rotated counterclockwise, with the length axis of the entire nanocrystal aligned horizontally. (c) Two-dimensional lattice model illustrating the high-index (730) facet. The model corresponds to the region indicated by the box in (b). (d) TEM image of a TOH Au−Pd core−shell nanocrystal viewed along the [1−10] axis. The inset shows the electron-diffraction pattern recorded on the nanocrystal. (e) HRTEM image of the region indicated by the orange rectangle in (d). (f) Two-dimensional lattice model illustrating the high-index (221) facet. The model corresponds to the region indicated by the red rectangle in (e).

The morphologies and high-index facets of the THH and TOH Pd nanoshells were maintained after one cycle of the catalytic reaction, as revealed by HRTEM imaging (Figure 6). The recycling capabilities of these samples were also examined by taking out the supernatant after the reaction and leaving the naturally precipitated nanocrystals for another cycle of the coupling reaction. High product yields of 86% were still obtained for the second cycle of the reaction.

CONCLUSION

We have demonstrated the heteroepitaxial growth of the Pd nanoshells on the high-index-faceted THH and TOH Au nanocrystals. The {730} and {221} facets of the THH and TOH Au nanocrystals are inherited by the grown Pd nanoshells. These high-index-faceted Pd nanoshells have been found to exhibit higher catalytic activities than Pd nanocubes that are enclosed with the low-index {100} facets for the Suzuki coupling reaction. The TONs per surface Pd atom of the Pd nanoshells are 3−7 times those of the Pd nanocubes. The higher catalytic performance of the Pd nanoshells is attributed to the presence of a large number of Pd atoms at steps on the high-index facets. The Pd atoms at steps, more coordinatively unsaturated than those on flat terraces, are more efficient in catalytically breaking the C−I bonds in the Suzuki coupling reaction. Our approach of using preformed high-index-faceted metal nanocrystals to heteroepitaxially direct the growth of high-index-faceted metal nanoshells with high catalytic activities points out a potential way for the design and preparation of inexpensive and highly active metal nanocatalysts.

ASSOCIATED CONTENT

Supporting Information. SEM and TEM images of the THH and TOH Au nanocrystals, THH and TOH Au−Pd

dx.doi.org/10.1021/ja1095733 |J. Am. Chem. Soc. 2011, 133, 1106–1111

core−shell nanocrystals, octahedral Au nanocrystals, Pd nanocubes, and Au−Pd core−shell nanocubes, and the calculation details of the total numbers of the surface Pd atoms of the four types of Pd-containing nanocrystals that were added in the coupling reaction. This material is available free of charge via the Internet at http://pubs.acs.org.

AUTHOR INFORMATION

Corresponding Author

jfwang@phy.cuhk.edu.hk; sun@pku.edu.cn; yan@pku.edu.cn

ACKNOWLEDGMENT

The work was supported in part by the Joint Research Scheme between National Natural Science Foundation of China and Hong Kong Research Grants Council (ref no., N_CUHK465/09; project code, 2900339) and National Natural Science Foundation of China (project codes: 20931160429 and 20828001).

REFERENCES

(1) Somorjai, G. A.; Li, Y. M. *Introduction to Surface Chemistry and Catalysis*, 2nd ed.; John Wiley & Sons: New Jersey, 2010.
(2) Somorjai, G. A. *Chem. Rev.* **1996,** *96*, 1223–1235.
(3) Li, Y. M.; Somorjai, G. A. *Nano Lett.* **2010,** *10*, 2289–2295.
(4) Feldheim, D. L. *Science* **2007,** *316*, 699–700.
(5) Somorjai, G. A.; Park, J. Y. *Angew. Chem., Int. Ed.* **2008,** *47*, 9212–9228.
(6) Nørskov, J. K.; Bligaard, T.; Hvolbæk, B.; Pedersen, F. A.; Chorkendorff, I.; Christensen, C. H. *Chem. Soc. Rev.* **2008,** *37*, 2163–2171.
(7) Zambelli, T.; Wintterlin, J.; Trost, J.; Ertl, G. *Science* **1996,** *273*, 1688–1690.
(8) Feibelman, P. J.; Esch, S.; Michely, T. *Phys. Rev. Lett.* **1996,** *77*, 2257–2260.
(9) Dahl, S.; Logadottir, A.; Egeberg, R. C.; Larsen, J. H.; Chorkendorff, I.; Törnqvist, E.; Nørskov, J. K. *Phys. Rev. Lett.* **1999,** *83*, 1814–1817.
(10) Yang, H. G.; Sun, C. H.; Qiao, S. Z.; Zou, J.; Liu, G.; Smith, S. C.; Cheng, H. M.; Lu, G. Q. *Nature* **2008,** *453*, 638–641.
(11) Inderwildi, O. R.; Jenkins, S. J.; King, D. A. *J. Am. Chem. Soc.* **2008,** *130*, 2213–2220.
(12) Lee, S. W.; Chen, S.; Sheng, W. C.; Yabuuchi, N.; Kim, Y.-T.; Mitani, T.; Vescovo, E.; Shao-Horn, Y. *J. Am. Chem. Soc.* **2009,** *131*, 15669–15677.
(13) Somorjai, G. A.; Park, J. Y. *Chem. Soc. Rev.* **2008,** *37*, 2155–2162.
(14) Bell, A. T. *Science* **2003,** *299*, 1688–1691.
(15) Van Santen, R. A. *Acc. Chem. Res.* **2009,** *42*, 57–66.
(16) Tsung, C.-K.; Kuhn, J. N.; Huang, W. Y.; Aliaga, C.; Hung, L.-I.; Somorjar, G. A.; Yang, P. D. *J. Am. Chem. Soc.* **2009,** *131*, 5816–5822.
(17) Zeng, J.; Zhang, Q.; Chen, J. Y.; Xia, Y. N. *Nano Lett.* **2010,** *10*, 30–35.
(18) Studt, F.; Pedersen, F. A.; Bligaard, T.; Sørensen, R. Z.; Christensen, C. H.; Nørskov, J. K. *Science* **2008,** *320*, 1320–1322.
(19) Schmidt, E.; Vargas, A.; Mallat, T.; Baiker, A. *J. Am. Chem. Soc.* **2009,** *131*, 12358–12367.
(20) Somorjai, G. A.; Blakely, D. W. *Nature* **1975,** *258*, 580–583.
(21) Ming, T.; Feng, W.; Tang, Q.; Wang, F.; Sun, L.-D.; Wang, J. F.; Yan, C.-H. *J. Am. Chem. Soc.* **2009,** *131*, 16350–16351.
(22) Ma, Y. Y.; Kuang, Q.; Jiang, Z. Y.; Xie, Z. X.; Huang, R. B.; Zheng, L. S. *Angew. Chem., Int. Ed.* **2008,** *47*, 8901–8904.
(23) Wu, H.-L.; Kuo, C.-H.; Huang, M. H. *Langmuir* **2010,** *26*, 12307–12313.
(24) Tian, N.; Zhou, Z.-Y.; Yu, N.-F.; Wang, L.-Y.; Sun, S.-G. *J. Am. Chem. Soc.* **2010,** *132*, 7580–7581.
(25) Tian, N.; Zhou, Z.-Y.; Sun, S.-G.; Ding, Y.; Wang, Z. L. *Science* **2007,** *316*, 732–735.
(26) Lu, C.-L.; Prasad, K. S.; Wu, H.-L.; Ho, J.-A.; Huang, M. H. *J. Am. Chem. Soc.* **2010,** *132*, 14546–14553.
(27) Fan, F.-R.; Liu, D.-Y.; Wu, Y.-F.; Duan, S.; Xie, Z.-X.; Jiang, Z.-Y.; Tian, Z.-Q. *J. Am. Chem. Soc.* **2008,** *130*, 6949–6951.
(28) Niu, W. X.; Li, Z.-Y.; Shi, L. H.; Liu, X. Q.; Li, H. J.; Han, S.; Chen, J. A.; Xu, G. B. *Cryst. Growth Des.* **2008,** *8*, 4440–4444.
(29) Xiang, Y. J.; Wu, X. C.; Liu, D. F.; Jiang, X. Y.; Chu, W. G.; Li, Z. Y.; Ma, Y.; Zhou, W. Y.; Xie, S. S. *Nano Lett.* **2006,** *6*, 2290–2294.
(30) Wang, F.; Sun, L.-D.; Feng, W.; Chen, H. J.; Yeung, M. H.; Wang, J. F.; Yan, C.-H. *Small* **2010,** *6*, 2566–2575.
(31) Kim, S.-W.; Kim, M.; Lee, W. Y.; Hyeon, T. *J. Am. Chem. Soc.* **2002,** *124*, 7642–7643.
(32) Chen, Y.-H.; Hung, H.-H.; Huang, M. H. *J. Am. Chem. Soc.* **2009,** *131*, 9114–9121.
(33) Li, C. C.; Sato, R.; Kanehara, M.; Zeng, H. B.; Bando, Y.; Teranishi, T. *Angew. Chem., Int. Ed.* **2009,** *48*, 6883–6887.